PERGAMON

International Journal of Heat and Mass Transfer 44 (2001) 2287–2297

International Journal of HEAT and MASS TRANSFER

www.elsevier.com/locate/ijhmt

Analysis of the operational characteristics and limits of a loop heat pipe with porous element in the condenser

I. Muraoka *, F.M. Ramos, V.V. Vlassov

Instituto Nacional de Pesquisas Espaciais, Caixa Postal 515, Av. dos Astronautas, 1758, 12227-010, São José dos Campos, SP, Brazil

Received 9 September 1999; received in revised form 25 July 2000

Abstract

This paper analyzes the operational characteristics and limits of a loop heat pipe (LHP) with flat porous elements in the condenser and evaporator. A mathematical model, based on the nodal method, was developed to simulate the thermal and hydrodynamic behavior of this specific type of LHP. Previously, the model was verified and validated by experiential data [I. Muraoka, F.M. Ramos, V. Vlassov, Int. Commun. Heat Mass Transfer 25 (1998) 1085]. The dry-out failure mechanisms of this device were investigated and its operational limits identified in terms of the heat load dissipated in the evaporator and the heat sink temperature at the condenser. Three distinct operational regimes were identified and characterized, taking into account the volume of vapor in the liquid core of the evaporator and the capillary pressure limit.

1. Introduction

Capillary pumped loop (CPL) and loop heat pipe (LHP) are two-phase heat-transport devices which rely on the surface-tension forces induced by a fine pore wick to drive a working fluid. These devices use the same basic principle of the widely known heat pipes, i.e., closed evaporation–condensation cycle being maintained by capillary pumping. The principal distinction is that both CPL and LHP have separate tube-type transport lines for vapor and liquid phases and the main porous structure is localized in the evaporator only. It allows to reduce drastically the hydraulic limit in the transport line and to provide a high capillary pressure. As their grand potential heat transport efficiency, these devices are emerging as the baseline design of thermal control systems for future spacecrafts.

CPLs were invented in USA (NASA) in late 1960s [2] whereas LHPs appeared in Russia in early 1970s [3,4]. These devices have the same basic operation principle, but were developed in parallel and independently. In spite of significant similarity, the difference in the origin explains partly the distinction in the terminology. Also these two devices have some distinct features due to different position and role of an additional reservoir (also named as hydro-accumulator or compensation cavity [5]), so at present they are treated as separate type devices. A review of CPL and LHP and their similarities and differences can be found in [5–7].

Both generic CPL and LHP have a cylindrical fine pore evaporator and a tube-type condenser. The CPL has a reservoir as a separate element having a hydraulic link to the liquid line, whereas in the LHP there is a compensation cavity which is incorporated in the evaporator. One of the functions of the reservoir in CPL, or compensation cavity in LHP, is to accommodate volume variations of the liquid phase in the condenser due to the liquid–vapor interface movements in response to variations in the heat input or in the environmental conditions. The CPL reservoir is also used for active control and for pre-conditioning at the start-up. Properly sized, the compensation cavity in LHP allows normal operation even with vapor in the evaporator entrance.

Although the CPL and LHP technologies have reached a high level of development, some issues still remain as points of active research. One of the main subjects of investigation is the occurrence of evaporator

* Corresponding author. Tel.: +55-12-345-6204; fax: +55-12-345-6226.

E-mail address: issamu@dem.inpe.br (I. Muraoka).

0017-9310/01/$ - see front matter
PII: S0017-9310(00)00259-3

Nomenclature

A	section area or interface area
C	conductive conductance
c_p	specific heat
D	diameter
F	fluid conductance
g	gravity acceleration
H	convective conductance
h	convective heat transfer coefficient
K	permeability
k	thermal conductivity
L	length
M	mass
$\dot{M}$	time variation of the fluid mass
$\dot{m}$	mass flow rate
N	total number of nodes
p	pressure
Q	heat flux
R	gas constant
r_{eff}	effective pore radius
T	temperature
t	time
V	volume
Δz	difference of level between evaporator and condenser

Greek symbols

δ	liquid layer thickness
λ	fluid latent heat
μ	fluid dynamic viscosity
ρ	fluid density
σ	fluid surface tension

Subscripts

bub	bubble
c	condenser
cap	capillary
cc	compensation cavity
cond	condensation process
e	evaporator
evap	evaporation process
f	fluid
hydr	hydrostatic
i, j	nodes
ij	between i and j or from i to j
l, ll	liquid, liquid line
loop	LHP entire circuit loop
plate	cold plate
s	saturation
sink	heat sink
v, vl	vapor, vapor line
w	wick

dry-out. It can happen during the CPL start-up, during operation, on attempting to re-start after temporary switch-off, or even during the reduction of heat input.

Start-up failures have been mainly studied experimentally [8–10], and are attributed to an unsuitable initial phase distribution inside the loop. Failures during operation may occur due to achieving of the capillary limit, insufficient sub-cooling in the condenser or after the onset of an instability process. High frequency pressure oscillation is related to the hydrodynamic interaction between the fluid reservoir and the CPL loop [11–13]. Low frequency oscillation is caused by the formation of a vapor bubble in the liquid core at the evaporator entrance [14,15]. Dry-outs on re-start have not been studied systematically in spite of their applicability relevance. The low power limit is mentioned in [5,7].

In this work, we present a complete study of the operational limits of a capillary pumped two-phase loop with a configuration simpler than a CPL or a LHP. It is a single heat transfer loop with porous elements in the condenser as well as in the evaporator. It does not have a separate reservoir like CPL and does not have a compensation cavity like LHP (more precisely, the liquid core and compensation cavity is the same in this device). For the porous condenser conception, the use of a reservoir to accommodate the liquid–vapor interface movement does not make sense. It can be seen as an intermediate device between HP and CPL/LHP. By Maidanik and Fershtater [5] it could be classified as a "separated lines heat pipe based on a loop scheme", but a flat disc conception of porous elements does not fit completely in this denomination. For the purpose of this paper we will call this device here as a specific type of loop heat pipe, keeping LHP as abbreviation. The liquid core below evaporator wick will be called the compensation cavity, following the LHP nomenclature, in spite of the fact that it does not execute all the functions it has in LHP.

The analysis of this specific LHP is accomplished using a mathematical model based on nodal method. The model was validated with experimental data obtained from testing of this device prototype [1]. The result of the present study can be also useful for CPL and conventional LHP because the vapor formation in the liquid core of evaporator is the only mechanism of dry-out failures, as mentioned above.

The paper is organized as follows. In Sections 2 and 3, we describe, respectively, the LHP in study and the mathematical model which simulates its thermal and hydrodynamic transient behavior. In Section 4, we study in detail the operational characteristics of this device as

well as the bubble formation mechanisms. Finally, in Section 5, we present the conclusions and the final remarks.

2. Description of the studied LHP

The LHP configuration studied in this work is schematically presented in Fig. 1. It is composed by an evaporator, a condenser, and the vapor and liquid lines. In contrast with the conventional CPL/LHP configuration, in the present design not only the evaporator but also the condenser are equipped with a wick structure. Also it does not have a separate reservoir like a CPL. The ideas behind this design are the following. The use of a wick structure in the condenser and the absence of a separate reservoir provide a stable physical interface between the liquid and the vapor phases in the condenser, reducing or even eliminating the possible occurrence of pressure oscillations during operation, like in a CPL. The use of a flat porous condenser provides a fixed sub-cooling as opposed to the tube-type condenser in conventional CPL/LHP, where the rate of sub-cooling is variable. The void below the evaporator wick arranges the liquid supply, as the liquid core in CPL/LHP evaporators, and also assists the operation with vapor at the evaporator entrance, as the compensation cavity in conventional LHP.

The functioning principle is similar to the conventional CPLs and LHPs. The studied device is charged with the working fluid in such a way that the liquid fills the pores of the wicks and all the volume below the wicks, comprising the liquid line and the compensation cavity (see Fig. 1). All the volume left above the wicks is occupied by the vapor. As heat is dissipated in the evaporator, the working fluid evaporates on the upper surface of the evaporator wick, creating meniscus on it, which prevents the vapor of penetrating inside the porous element. The vapor then flows to the condenser, through the vapor line, where it condenses in contact with the wick surface, which is cooled by the heat sink. The liquid is then sub-cooled as it passes through the condenser wick, and returns to the evaporator through the liquid line.

For the purpose of verifying the performance of this specific LHP and validating the proposed mathematical model, a prototype was built and tested. Some parts were made of transparent glass in order to allow the visualization of the phase distribution inside the loop and to detect the formation of bubbles in the compensation cavity. Disk shaped porous elements, made of sintered bronze, were used in the evaporator ($\varnothing 100$ mm $\times$ 10 mm, $r_{\text{eff}} = 35$ μm, $k = 15$ W/m K) and condenser ($\varnothing 100$ mm $\times$ 7 mm, $r_{\text{eff}} = 210$ μm, $k = 8$ W/m K). The vapor and liquid lines were made of stainless steel, measuring 1100 mm in length and 4.35 mm inner diameter. The prototype was charged with 138 ml of ethanol. As the purpose was not to obtain a high performance device, the wick material and working fluid were chosen by easy feasibility criteria. During the tests of this prototype, the cold plate was heated electrically using a skin-heater and the temperature of the heat sink was controlled by an external thermal-stabilized water loop. Experimental results are presented in [1].

3. Mathematical formulation

We developed a mathematical model for describing the transport of heat and mass inside the loop during all its operational regimes. This model comprises two different modules. The thermal module, which computes the distribution of temperatures as a function of time, is based on the nodal method [16]. Each node is characterized by a thermal capacitance, and is connected to other nodes by means of generalized thermal conductances. The hydrodynamic module determines the pressure and phase distributions inside the loop, as well as the flow rates of liquid and vapor.

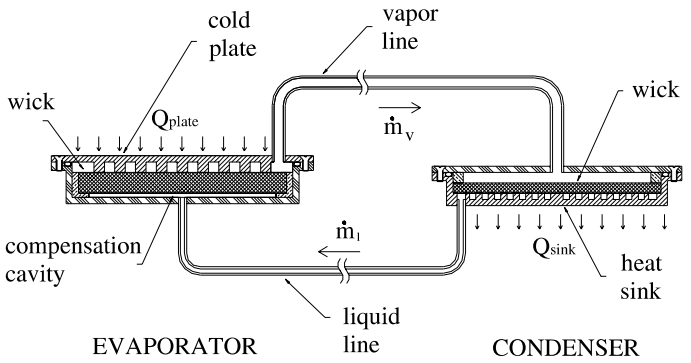

Fig. 1. Sketch of the proposed device.

The thermal and hydrodynamic systems are coupled since, on the one hand, the transport of heat depends on the fluid flow, on the other hand, the pressure distribution, that drives the fluid along the loop, is a function of the temperature distribution. This mathematical model was validated using experimental data, as presented in [1].

3.1. Thermal module

The temperature distribution is determined by solution of a system of ordinary differential equations. Each equation represents the thermal balance at the nodal level, and is given by

$$M_i c_{P_i} \frac{\mathrm{d}T_i}{\mathrm{d}t} = \sum_{j=1}^{N} C_{ji}(T_j - T_i) + \sum_{j=1}^{N} H_{ji}(T_j - T_i) + \sum_{j=1}^{N} F_{ji}(T_j - T_i) + Q_i, \quad i = 1, \ldots, N. \tag{1}$$

The conductive, convective, and fluid conductances are calculated, respectively, by

$$C_{ji} = \frac{k_{ji} A_{ji}}{L_{ji}}, \quad H_{ji} = h_{ji} A_{ji} \quad \text{and} \quad F_{ji} = \dot{m}_{ji} c_{P,f}. \tag{2}$$

Q_i models the heat load dissipated at the evaporator, and also the latent heat released by the vapor at the condenser or absorbed at the evaporator, respectively

$$\begin{aligned} Q_i &= +\dot{m}_\mathrm{v}\lambda, \quad i = \text{condenser} \quad \text{and} \\ Q_i &= -\dot{m}_\mathrm{v}\lambda, \quad i = \text{evaporator}. \end{aligned} \tag{3}$$

The mass flow rates $\dot{m}_\mathrm{v}$ and $\dot{m}_{ji}$ depend on the pressure distribution computed by the hydrodynamic module.

3.2. Hydrodynamic module

3.2.1. Maximum pumping pressure and flow rates

The maintenance of a continuous flow of fluid is assured by capillary pressure of the evaporator wick. Hence, a basic condition for the device operation is that the total pressure loss along the loop shall not surpass the maximum capillary pressure of the evaporator wick, i.e.,

$$\Delta p_\mathrm{loop} \leqslant \Delta p_\mathrm{cap,max} \quad \text{with} \quad \Delta p_\mathrm{cap,max} = 2\sigma / r_\mathrm{eff}. \tag{4}$$

The total pressure loss in the loop is given by the summation of losses in each component along the circuit, as follows:

$$\Delta p_\mathrm{loop} = \Delta p_\mathrm{vl} + \Delta p_\mathrm{ll} + \Delta p_\mathrm{w,e} + \Delta p_\mathrm{w,c} + \Delta p_\mathrm{evap} + \Delta p_\mathrm{cond} + \Delta p_\mathrm{hydr}. \tag{5}$$

Assuming that the vapor is saturated at the evaporator and the condenser, the pressure loss in the vapor line is given by

$$\Delta p_\mathrm{vl} = p_\mathrm{s}(T_\mathrm{e}) - p_\mathrm{s}(T_\mathrm{c}), \tag{6}$$

where $p_\mathrm{s}(T_\mathrm{e})$ and $p_\mathrm{s}(T_\mathrm{c})$ are the saturation pressures of the vapor at the evaporation and condensation temperatures, respectively.

Assuming laminar flow conditions, the pressure loss in the liquid line and the hydrostatic pressure are, respectively, given by

$$\Delta p_\mathrm{ll} = \frac{128 \mu_\mathrm{l} \dot{m}_\mathrm{l} L_\mathrm{ll}}{\pi \rho_\mathrm{l} D_\mathrm{ll}^4} \quad \text{and} \quad \Delta p_\mathrm{hydr} = \rho_\mathrm{l} g \Delta z, \tag{7}$$

where Δz is the height difference between the evaporator and the condenser. The pressure losses, due to the passage of the liquid through the evaporator and the condenser wicks, are calculated by the equations derived from Darcy's law, that are

$$\Delta p_\mathrm{w,e} = \frac{\mu_\mathrm{l} \dot{m}_\mathrm{l} L_\mathrm{w,e}}{K_\mathrm{w,e} A_\mathrm{w,e} \rho_\mathrm{l}} \quad \text{and} \quad \Delta p_\mathrm{w,c} = \frac{\mu_\mathrm{l} \dot{m}_\mathrm{l} L_\mathrm{w,c}}{K_\mathrm{w,c} A_\mathrm{w,c} \rho_\mathrm{l}}. \tag{8}$$

The pressure losses during the process of phase change are given by

$$\begin{aligned} \Delta p_\mathrm{evap} &= \frac{\dot{m}_\mathrm{v}}{A_\mathrm{evap}} \sqrt{2\pi R_\mathrm{v} T_\mathrm{v}} \quad \text{and} \\ \Delta p_\mathrm{cond} &= \frac{\dot{m}_\mathrm{v}}{A_\mathrm{cond}} \sqrt{2\pi R_\mathrm{v} T_\mathrm{v}}. \end{aligned} \tag{9}$$

The vapor flow rate is calculated by an expression derived from the frictional resistance in smooth pipes of circular cross-section for a turbulent flow [17], which results in

$$\dot{m}_\mathrm{v} = \left(\frac{\Delta p_\mathrm{vl} D_\mathrm{vl}^{4.75} \rho_\mathrm{v}}{0.241 \mu_\mathrm{v}^{0.25} L_\mathrm{vl}} \right)^{1/1.75}. \tag{10}$$

If there is no bubble generation, the mass flow rate can be assumed to be uniform along the circuit, i.e.,

$$\dot{m}_\mathrm{l} = \dot{m}_\mathrm{v}. \tag{11}$$

Otherwise, a correction shall be introduced in the model, as described in the following section.

3.2.2. Bubble formation at the compensation cavity

Under certain operation conditions, vapor bubbles appear below the evaporator wick, i.e., in the compensation cavity (see Fig. 1). This phenomenon strongly affects the device behavior because it induces the formation of a liquid layer on the upper surface of the condenser wick. Since the thermal conductivity of the working fluid is relatively low, this liquid layer acts as a thermal barrier between the vapor and heat sink, and increases the device overall thermal resistance. In the limit, the bubble growing can lead to a obstruction of the liquid flow at the entrance of the evaporator, causing the dry-out.

In addition, with the expansion or reduction of the bubble volume, the mass flow rate is no longer described

by Eq. (11). The process of bubble formation depends on the temperature and the pressure of the liquid inside the compensation cavity. In steady-state operation, with presence of bubble in the compensation cavity, the following expression can be applied to the device:

$$\Delta p_{\text{loop}} - \Delta p_{\text{w,e}} = p_{\text{s}}(T_{\text{e}}) - p_{\text{s}}(T_{\text{cc}}), \tag{12}$$

where the equality $p_{\text{cc}} = p_{\text{s}}(T_{\text{cc}})$ is implicit. The change of the bubble volume occurs when a disturbance in the system deviates p_{cc} from $p_{\text{s}}(T_{\text{cc}})$.

The variation of the vapor mass inside the bubble can be expressed as

$$\dot{M}_{\text{bub,v}} = A_{\text{bub}}\sqrt{\frac{1}{2\pi R_{\text{v}} T_{\text{cc}}}}[p_{\text{s}}(T_{\text{cc}}) - p_{\text{cc}}]. \tag{13}$$

Hence, the variation of the fluid mass inside the compensation cavity, supposing that the vapor mass is small compared to the liquid mass, can be expressed as $\dot{M}_{\text{cc}} = -\dot{M}_{\text{bub,v}}\rho_{\text{l}}/\rho_{\text{v}}$. This mass variation corresponds to the mass of liquid that is displaced by the bubble and that will eventually accumulate on the condenser wick. Assuming that the vapor flow rate is not affected by bubble formation, the liquid flow rate is given by

$$\begin{aligned}\dot{m}_{\text{l}} &= \dot{m}_{\text{v}} + \dot{M}_{\text{cc}} \\ &= \dot{m}_{\text{v}} - \frac{\rho_{\text{l}}}{\rho_{\text{v}}} A_{\text{bub}}\sqrt{\frac{1}{2\pi R_{\text{v}} T_{\text{cc}}}}[p_{\text{s}}(T_{\text{cc}}) - p_{\text{cc}}].\end{aligned} \tag{14}$$

The pressure at the compensation cavity, p_{cc}, can be obtained from the pressure at the condenser taking into account the losses between the condenser and the compensation cavity, as follows:

$$p_{\text{cc}} = p_{\text{s}}(T_{\text{c}}) - \Delta p_{\text{cond}} - \Delta p_{\text{w,c}} - \Delta p_{\text{ll}} - \Delta p_{\text{hydr}}. \tag{15}$$

Expressing Δp_{ll} and $\Delta p_{\text{w,c}}$ as functions of $\dot{m}_{\text{l}}$, as presented in Eqs. (7) and (8), and introducing the result into Eq. (15) and then into Eq. (14), the following relation for liquid flow rate can be obtained after some arrangements:

$$\dot{m}_{\text{l}} = \frac{\dot{m}_{\text{v}} + A_{\text{bub}}(\rho_{\text{l}}/\rho_{\text{v}})\sqrt{1/2\pi R_{\text{v}} T_{\text{cc}}}\left[p_{\text{s}}(T_{\text{c}}) - p_{\text{s}}(T_{\text{cc}}) - \Delta p_{\text{cond}} - \Delta p_{\text{hydr}}\right]}{1 + A_{\text{bub}}\rho_{\text{l}}/\rho_{\text{v}}\sqrt{1/2\pi R_{\text{v}} T_{\text{cc}}}(128\mu_{\text{l}} L_{\text{ll}}/\rho_{\text{l}} D_{\text{ll}}^2) + (\mu_{\text{l}} L_{\text{w,c}}/K_{\text{w,c}} A_{\text{w,c}}\rho_{\text{l}})}. \tag{16}$$

As Eq. (16) does not consider the limit of the capillary pressure, the liquid flow rate, calculated by it, may result in the unrealistic condition $\Delta p_{\text{loop}} > \Delta p_{\text{cap,max}}$. In this case, the liquid flow rate should be recalculated considering

$$\Delta p_{\text{c,max}} = \Delta p_{\text{loop}}. \tag{17}$$

Introducing Eqs. (5), (7)–(9) in (17), we obtain the following equation for the liquid flow rate, for the device operating with the capillary limit:

$$\dot{m}_{\text{l}} = \frac{\Delta p_{\text{c,max}} - \Delta p_{\text{vl}} - \Delta p_{\text{cond}} - \Delta p_{\text{evap}} - \Delta p_{\text{hydr}}}{(\mu_{\text{l}}/\rho_{\text{l}})((128 L_{\text{ll}}/D_{\text{ll}}^2) + (L_{\text{w,c}}/K_{\text{w,c}} A_{\text{w,c}}) + (L_{\text{w,e}}/K_{\text{w,e}} A_{\text{w,e}}))}. \tag{18}$$

The difference between the flow rate of vapor and liquid results in a variation of the bubble volume and of the thickness of the liquid layer accumulated on the upper surface of the condenser wick. The variation of the bubble volume between time steps t and $t + \Delta t$ can be calculated by

$$\begin{aligned}&\Delta V_{\text{bub}} = \frac{\dot{m}_{\text{v}} - \dot{m}_{\text{l}}}{\rho_{\text{v}}}\Delta t \quad \text{with} \\ &(V_{\text{bub}})_{t+\Delta t} = (V_{\text{bub}})_t + \Delta V_{\text{bub}}.\end{aligned} \tag{19}$$

Similarly, the variation of liquid layer thickness is given by

$$\Delta\delta = \frac{\dot{m}_{\text{v}} - \dot{m}_{\text{l}}}{\rho_{\text{l}} A_{\text{w,c}}}\Delta t \quad \text{with} \quad (\delta)_{t+\Delta t} = (\delta)_t + \Delta\delta. \tag{20}$$

This liquid layer represents an additional thermal resistance between the surface of condensation and the condenser wick element, and its conductance is given by

$$C_{ji} = \frac{k_{\text{l}} A_{\text{w,c}}}{\delta}. \tag{21}$$

This layer contributes to a self-regulation mode of this specific LHP.

4. Device operational characteristics and limits

The steady-state behavior of the loop was simulated under different conditions of imposed heat load, at the evaporator, and heat sink temperature at the condenser. Results, summarized in Fig. 2, allow us to identify five regions, representing distinct operational regimes. These regions are defined in terms of (i) the generation or not of vapor bubbles at the compensation cavity, (ii) the total pressure loss along the circuit, compared to the capillary limit, and (iii) the occurrence or not of dry-out. Table 1 presents the characteristics of each region.

Curves 1 and 2 in Fig. 2 define the operational limits of the proposed LHP. The operation is impossible at any point situated inside regions *A* and *B*. For example, the loop will always dry-out when the heat sink temperature is below 10°C. This limitation is due to the small value of $\mathrm{d}p/\mathrm{d}T$ of the ethanol saturation curve, at low temperatures, and the relatively high thermal conductance of the evaporator porous element that, according to Eq. (12), define the pressure loss permitted in the loop. As another example, if the heat sink is at 20°C the operation is restricted to heat loads ranging from 91 to 133 W. The minimum of 91 W is also due to the properties of the working fluid and the porous element, as mentioned before. The maximum of 133 W is the limit imposed by

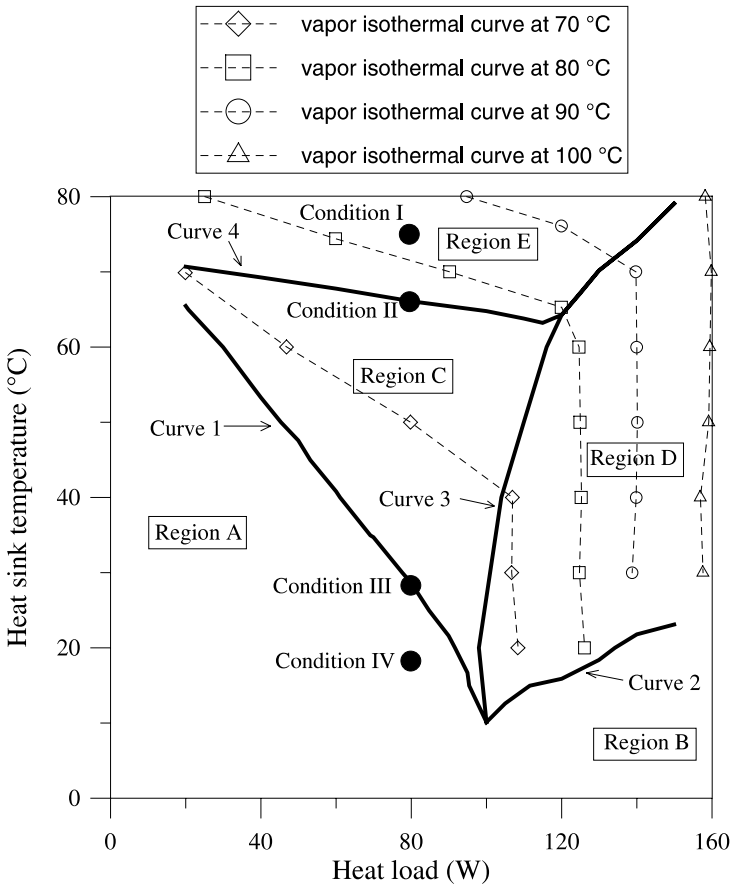

Fig. 2. Operational characteristics of the analyzed LHP.

the maximum capillary pressure of the evaporator porous element.

Curve 2 represents the restriction imposed by the capillary pumping limit of the evaporator wick. Below this curve (region B), the capillary pressure is not sufficient to pump, along the loop, the amount of fluid consumed in the evaporation process. The maximum transportable heat increases with the heat sink temperature, indicated by the positive inclination of Curve 2. It occurs because the vapor properties change favorably when the temperature increases, allowing a larger vapor flow rate, with the same pumping pressure.

Curve 1, in turn, defines the limits imposed by the temperature and pressure levels inside the compensation cavity. At the left side of this curve (region A), the bubble grows because the equilibrium stated in Eq. (12) cannot be reached, that is, the difference $p_s(T_e) - p_s(T_{cc})$ cannot be large enough to compensate the total pressure loss in the loop. Three main factors contribute to this condition: (i) the small heat load that generates insufficient sub-cooled liquid flow into the compensation cavity to reduce T_{cc} related to T_e; (ii) low working temperature that leads to a small value of dp/dT of the fluid saturation curve; (iii) high wick conductance that reduces the difference between T_e and T_{cc}.

Table 1
Characteristics of operation at each region of the diagram of Fig. 2

Region	Dry-out occurrence	Bubble generation	Total pressure loss
A	Yes	–	–
B	Yes	–	–
C	No	Yes	$\Delta p_{loop} < \Delta p_{cap,max}$
D	No	Yes	$\Delta p_{loop} = \Delta p_{cap,max}$
E	No	No	$\Delta p_{loop} < \Delta p_{cap,max}$

The appearance of bubbles in the compensation cavity does not necessarily interrupt the device operation. Failure occurs only when the bubble volume grows above a certain value and blocks the liquid flow into evaporator. In regions C and D, for example, in spite of the presence of bubbles, the device operates normally. In these conditions Eq. (12) is applicable when the operation reaches the steady state.

In region C, where the total pressure loss in the loop is below the capillary limit, the equilibrium, stated by Eq. (12), is reached in function of the variation of the bubble volume. When, due to an external disturbance, the difference $p_s(T_e) - p_s(T_{cc})$ becomes momentarily smaller than $\Delta p_{loop} - \Delta p_{w,e}$, the pressure at compensation cavity becomes lower than saturation pressure, that is, $p_{cc} < p_s(T_{cc})$. This condition causes the bubble growing that increases the device overall thermal resistance, lifting the vapor temperature. As consequence (i) the local derivative dp/dT of saturation curve becomes larger, (ii) the level of sub-cooling increases and (iii) the change in the vapor properties reduces the pressure loss in vapor line. These factors make the right-hand side of Eq. (12) to increase and the left-hand side to decrease, until a new equilibrium point is reached. In this region, the liquid flow is governed by Eq. (16).

In region D, the bubble appears because, even at its maximum value, the pumping pressure is not enough to circulate the necessary fluid to transport the heat imposed in the evaporator. As the bubble grows the device overall thermal resistance increases, lifting the fluid temperature. Due to the change in the fluid properties, caused by the fluid heating, it becomes possible to transport more fluid with the same pumping pressure. Eventually, the equilibrium is reached when the fluid reaches a temperature level that makes possible to transport the imposed heat with the maximum capillary limit. In this region, the liquid flow rate is determined by Eq. (18).

In region E, the boundary conditions allow the device to operate without any bubble, that is, the liquid in the compensation cavity is cooler than the respective saturation temperature, $p_{cc} > p_s(T_{cc})$, and the pressure loss in the loop is smaller than the capillary limit. In this case, the liquid flow is governed by Eqs. (11) and (12) is not valid.

In summary, the existence of all these operation modes is basically associated with the following factors: (i) the local inclination of the working fluid saturation curve; (ii) the total pressure loss along the loop; and (iii) the vapor bubble size and the corresponding amount of liquid accumulated as a layer above the upper surface of the condenser wick. The influence of each factor is detailed in the following sections.

Finally, the vapor isothermal curves, displayed in Fig. 2, gives the temperature of the vapor corresponding to each combination of heat sink temperature and heat load. This means, for example, that if the heat load is 80 W and heat sink is at 50°C, the vapor temperature, in steady-state operation, will be 70°C. In region D, due to effect of device variable conductance, the vapor temperature becomes practically independent of the heat sink temperature.

4.1. Operation with pumping pressure below the capillary limit

When the device operates with Δp_{loop} below $\Delta p_{cap,max}$ (regions C and E), the process of bubble formation only depends on the temperature and pressure levels inside the compensation cavity, and which side of the working fluid saturation curve – liquid or vapor – these conditions correspond to, as depicted in Fig. 3.

While at the upper face of the evaporator wick the working fluid conditions are always those given by its saturation curve (point A), since the liquid is evaporating at this place, the temperature and pressure levels inside the compensation cavity (point B) depend on the total pressure loss along the loop ($\Delta p = \Delta p_{loop} - \Delta p_{w,e}$) and the temperature difference between the upper face of the evaporator wick and the compensation cavity ($\Delta T = T_e - T_{cc}$).

The pressure difference Δp is directly proportional to the flow rate in the loop and hence, Δp remains constant for a given heat load at the evaporator. The temperature difference varies from ΔT_{min} to ΔT_{max}, as a function of the level of sub-cooling attained by the fluid as it passes through the condenser. The temperature difference is minimum when there is no bubble and, thus, no liquid layer accumulated on the condenser wick. ΔT_{max} is reached when V_{bub} and δ attain their maximum size, and dry-out occurs.

To explain the process of bubble formation at the compensation cavity, we consider the device operating at condition I and slowly passes through conditions II–IV, keeping the heat dissipation on the cold plate constant, as shown in Figs. 2 and 3. In condition I, there is no occurrence of bubbles because, at this temperature, the saturation curve is steep enough to keep the coordinates of the point B at the liquid side, even with ΔT_{min} (no liquid layer on the condenser wick).

As T_{sink} is reduced from condition I to II, the temperature of point A decreases and point B approaches the boundary between the liquid and vapor regions (eventually reaching it at the condition II), due to the reduction of the inclination of the saturation curve. At this point, bubbles begin to form in the compensation cavity, displacing an equivalent volume of liquid. This process results in the appearance of a liquid layer on the condenser wick which increases ΔT, by enhancing the sub-cooling in the condenser, and forces point B back to the saturation curve, where an equilibrium is reached.

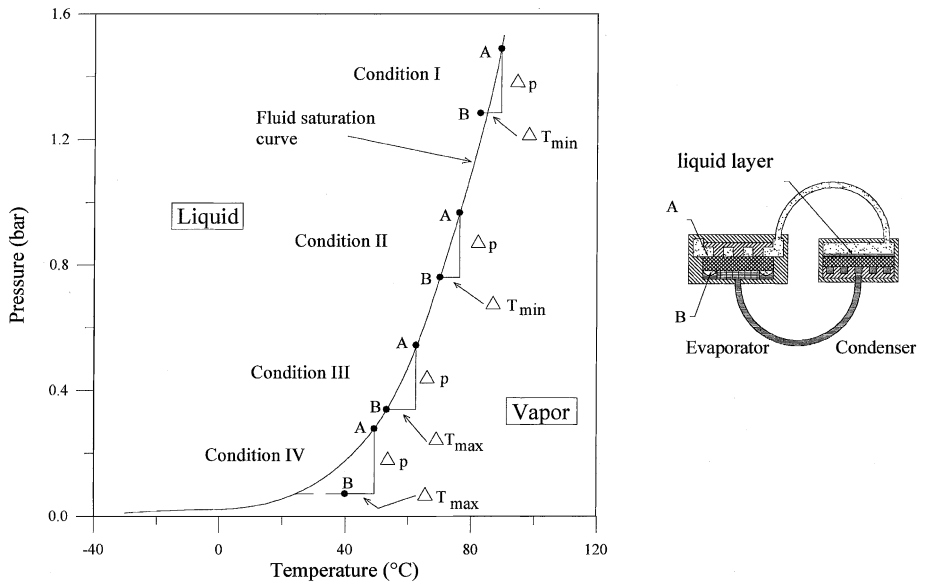

Fig. 3. Position of the temperature and pressure of the points A and B, related to the fluid saturation curve.

As T_{sink} is reduced from condition II to III, V_{bub} and δ continue to increase. Condition III represents the limit situation. Beyond this point, the inclination of the saturation curve becomes so small that, even with increasing values of ΔT, it is impossible to reach an equilibrium. In this case, condition IV for example, point B stays at the vapor side of the saturation curve and the bubble increases continually, resulting in the device dry-out.

4.2. Operation with pumping pressure equal to the capillary pressure limit

It seems paradoxical that it is possible to operate the device and, moreover, to increase the heat load transported by it, even when the loop is already working at the maximum capillary pressure. The reason for this relies on the fact that, for a given duct geometry and a fixed pumping pressure, the vapor flow rate is proportional to the relation $(\rho/\mu^{0.25})^{1/1.75}$ (see Eq. (10)). For ethanol, the working fluid used in the present study, this expression is a growing function of the temperature.

As the heat load is increased and total pressure drop reaches the maximum capillary pressure (region D), there is an internal compensation mechanism that automatically sets the vapor temperature, through bubble formation and liquid accumulation on the condenser wick, that allows to increase the heat transport while keeping Δp_{loop} equal to $\Delta p_{cap,max}$. This mechanism can be explained as follows. Keeping T_{sink} constant, any increase on Q_{plate} requires a larger $\dot{m}_v$. Since the pumping pressure is at its limit value, this causes a deficit of liquid in the evaporator, increasing the bubble volume in the compensation cavity and the liquid layer in the condenser. This, in turn, increases the thermal resistance between the vapor and the heat sink, and raises the vapor temperature at the condenser. The equilibrium is reached when T_v is high enough to make possible to transport Q_{plate} with $\Delta p_{loop} = \Delta p_{cap,max}$. The operation fails when it is not possible to further increase the vapor temperature, which happens when the bubble completely fills the compensation cavity and blocks the liquid flow into the evaporator. This condition is represented by Curve 2.

Also in region D, for each heat load, there is a minimum value for the vapor temperature that becomes possible to transport this Q_{plate} with $\Delta p_{loop} = \Delta p_{cap,max}$. If Q_{plate} is kept constant and the heat sink temperature is changed, the liquid layer thickness changes in a way to keep the vapor temperature constant, equal to the mentioned minimum value. This behavior is illustrated by the vapor isothermal lines in the vertical position, in region D of Fig. 2.

4.3. Simulation of operation with constant heat input and variable heat sink temperature

To illustrate the behavior of the device in its various operation regimes, results of two simulations with constant heat load (80 and 140 W) and variable heat sink temperature are presented. The variation of T_{sink} is sufficiently slow to the operation be considered in steady state at any time of the simulation. Results are presented in Figs. 4 and 5, respectively.

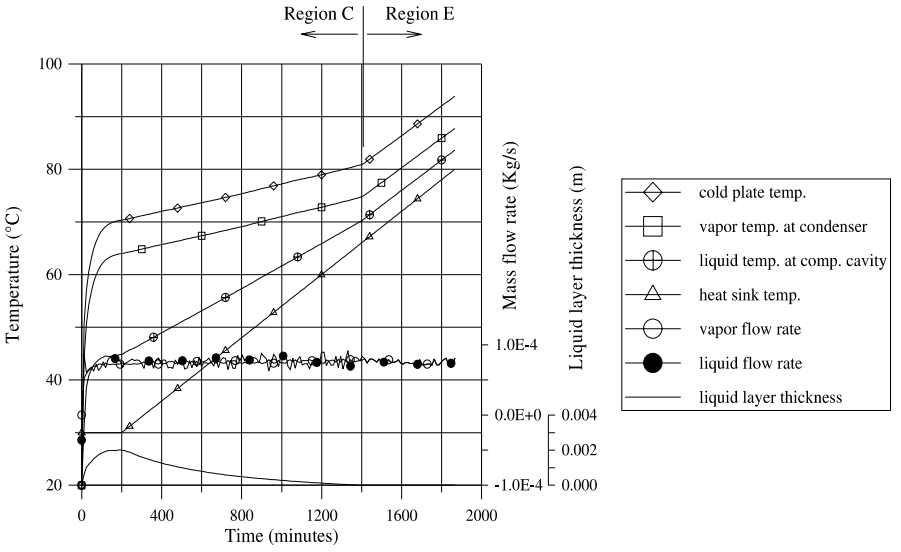

Fig. 4. Device behavior with constant heat input of 80 W and variable heat sink temperature from 30°C to 80°C.

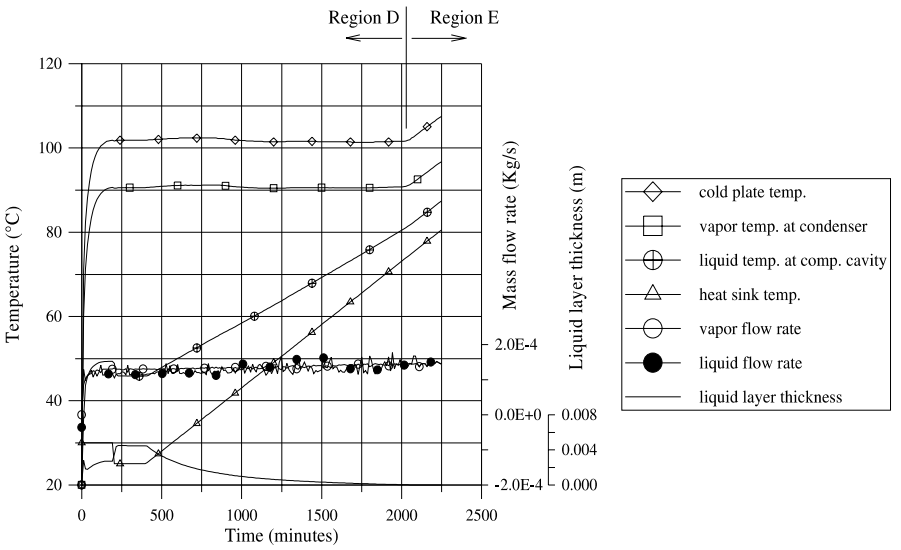

Fig. 5. Device behavior with constant heat input of 140 W and variable heat sink temperature from 25°C to 80°C.

In Fig. 4, after the start-up with the heat sink temperature of 30°C, we observe that as T_{sink} increases, the thickness of the liquid layer decreases, reducing the thermal resistance of the system, and consequently decreasing the influence of T_{sink} variation on the cold plate temperature. This behavior represents a process of self-regulation that tends to keep approximately constant the cold plate temperature at the evaporator, regardless of the heat sink temperature at the condenser. For T_{sink} higher than 66°C ($t \geqslant 1400$ min), when the operation conditions cross Curve 4 (at condition II), δ becomes null, the system looses its self-regulation capacity, and the cold plate temperature begins to increase at the same rate of T_{sink}.

A similar behavior is observed in the simulation with Q_{plate} of 140 W. In this case, the cold plate temperature remains almost constant, in spite of the change of T_{sink} from 25°C to 74°C. This behavior is explained by the fact that, in such condition, the device is working in region D, where the total pressure loss is equal to the maximum capillary pressure. The increase of T_{sink} is automatically compensated by a reduction of the liquid

layer on the condenser wick and the correspondent thermal resistance, keeping the vapor temperature constant. By explanation of Section 4.2, we can say that the vapor should be at a minimum of about 90°C to be possible to transport 140 W with $\Delta p_{loop} = \Delta p_{cap,max}$. This phenomenon was observed experimentally and presented in [1].

We also notice that in the regions of self-regulation, $\dot{m}_l$ oscillates around $\dot{m}_v$, indicating the fluctuation of the volume of the vapor bubble in the compensation cavity. These oscillations, observed experimentally [15], occur in the process of reaching the equilibrium between the bubble volume and vapor temperature. For higher heat sink temperatures, when there is no bubble formation (region E), the liquid and vapor flow rates coincide.

4.4. Simulation of operation with constant heat sink temperature and variable heat input

We also simulated the device operation with constant heat sink temperature (30°C) and variable heat load. The results are displayed in Fig. 6. After the start-up with Q_{plate} equal to 80 W, the bubble volume and the amount of liquid accumulated on the condenser entrance decrease as the heat load is slowly increased, until they reach a minimum for Q_{plate} equal to 100 W ($t = 900$ min), when the operation conditions cross Curve 3 of Fig. 2. From this point, the device begins to operate at the maximum capillary pressure and the previous tendency reverses.

In region D, V_{bub} grows and δ increases with the heat load, as described in Section 4.2 and illustrated by the corresponding curve of Fig. 6, for $t > 900$ min. When the bubble attains a volume that blocks the flow of liquid into the evaporator, dry-out occurs ($t = 3160$ min, $Q_{plate} = 170$ W).

5. Conclusions

In this work, we analyzed the operational characteristics and limits of a specific type of LHP with a porous element in the condenser. For this, we developed a system-level mathematical model capable to simulate dynamically the thermal and hydrodynamic behavior of the device. The model also allows to simulate in detail the process of bubble formation in the compensation cavity, which is an issue of fundamental importance for the overall performance of the studied device.

We determined the operational limits of the device, as a function of the heat load, at the evaporator, and the heat sink temperature, at the condenser. Also, the mechanisms of failure at different operational modes were investigated. In our simulations, we identified three regions where the device can operate properly (regions C, D and E of Fig. 2), and two regions (A and B) where operation fails. Each region has its own operational characteristics, in terms of the total pressure loss in the circuit (and its relation with the maximum capillary pressure) and the formation or not of vapor bubbles in the loop.

The operation of the studied device can coexist with vapor bubbles in the compensation cavity, as far as their size is not enough to block the liquid flow into evaporator. Bubbles are generated by effect of insufficient sub-cooling at the condenser, or by the combination of a relatively high temperature and low pressure in the compensation cavity at the evaporator. They promote a

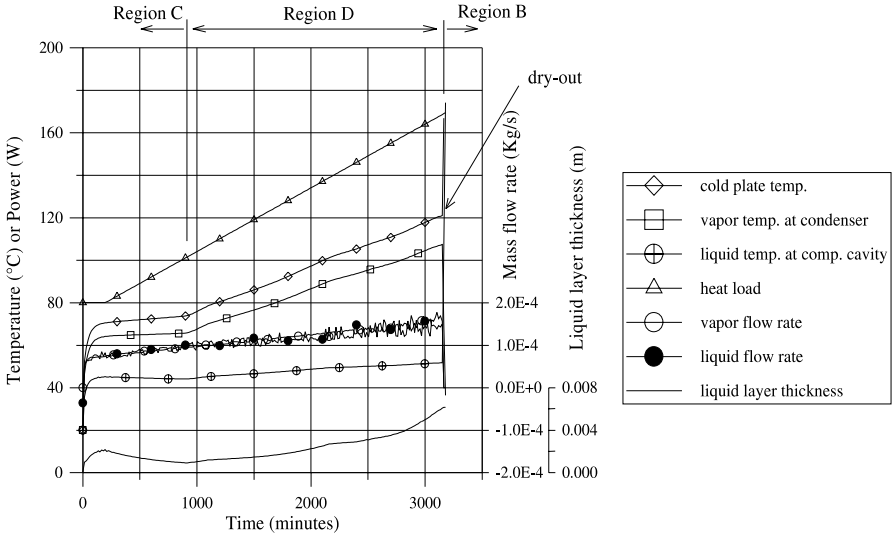

Fig. 6. Device behavior with constant heat sink temperature of 30°C and variable heat load from 80 to 168 W.

redistribution of fluid inside the loop that changes the device thermal resistance, inducing a type of self-regulation mechanism. This variable-conductance mode of operation keeps the cold plate temperature approximately constant in spite of variation of the heat input and the heat sink temperature. The discovered mechanism of self-regulation by a variable thickness liquid layer above the porous condenser surface is new and may have an important practical significance.

Although this study was done for a specific model of LHP, many of the qualitative conclusions about limits and characteristics of the operation, as well as the mechanism of the vapor bubble formation in the liquid core, can be applied to other types of CPL/LHP, since the dry-out failures are essentially related to the blockage of evaporator liquid supply, by vapor bubbles.

Acknowledgements

This work was supported by CNPq-Brazil, through research grants 523859/95-3 and 300171/97-8.

References

[1] I. Muraoka, F.M. Ramos, V. Vlassov, Experimental and theoretical investigation of a capillary pumped loop with a porous element in the condenser, Int. Commun. Heat Mass Transfer 25 (1998) 1085–1094.

[2] F.J. Stenger, Experimental feasibility study of water-filled capillary-pumped heat-transfer loops, NASA TM X-1310, NASA, Washington, D.C., 1966.

[3] Y.F. Gerasimov, Y.F. Maidanik, Y.Y. Dolgirev, et al., Some results of investigation of low-temperature heat pipes operating against gravity field, Eng. Phys. J. 30 (4) (1976) 581–586 (in Russian).

[4] Y.F. Maidanik, S. Vershinin, V. Kholodov, J. Dolgirev, US Patent No. 4515209, 1985.

[5] Y.F. Maidanik, Y.G. Fershtater, Theoretical basis and classification of loop heat pipes and capillary pumped loops, in: Proceedings of the 10th International Heat Pipe Conference, Stuttgart, Germany, 1997.

[6] M. Nikitkin, B. Cullimore, CPL and LHP technologies: what are the differences, what are the similarities, SAE Paper 981587, in: Proceedings of the 28th International Conference on Environmental Systems, Danvers, MA, 1998.

[7] J. Ku, Operating characteristics of loop heat pipes, SAE Paper 99-01-2007, in: Proceedings of the 29th International Conference on Environmental Systems, Denver, CO, 1999.

[8] Y. Maidanik, Y. Fershtater, V.G. Pastukhov, M. Chernysheva, Experimental and theoretical investigation of startup regimes of two-phase capillary pumped loops, SAE paper 932305, in: Proceedings of the 23rd International Conference on Environmental Systems, Colorado Springs, CO, 1993.

[9] R. Meyer, R. Muller, K. Beckmann, K.A. Goncharov, E.Y. Kotlyarov, Y.F. Maidanik, Investigation of the heat transfer performance of a capillary pumped ammonia loop under gravity, SAE paper 932304, in: Proceedings of the 23rd International Conference on Environmental Systems, Colorado Springs, CO, 1993.

[10] J. Ku, T. Hoang, T. Nguyen, S. Yun, Performance tests of CAPL2 starter pump cold plates, AIAA paper 96-1837, in: Proceedings of the 31st AIAA Thermophysics Conference, New Orleans, LA, 1996.

[11] T. O'Connell, T. Hoang, J. Ku, Investigation of power turn down transients in CAPL-1 flight experiment, AIAA paper 95-2067, in: Proceedings of the 30th AIAA Thermophysics Conference, San Diego, CA, 1995.

[12] J. Ku, T. Hoang, An experimental study of pressure oscillation and hydrodynamic stability in a Capillary Pumped Loop, in: Proceedings of the ASME National Heat Transfer Conference, Portland, OR, vol. 5, 1995, pp. 25–32.

[13] T. Hoang, J. Ku, Theory of hydrodynamic stability for capillary pumped loops, in: Proceedings of the ASME National Heat Transfer Conference, Portland, OR, vol. 5, 1995, pp. 33–40.

[14] K.R. Kolos, K.E. Herold, Low frequency temperature and fluid oscillations in capillary pumped loops, AIAA paper 97-3872, in: Proceedings of National Heat Transfer Conference, Baltimore, MD, 1997.

[15] I. Muraoka, F.M. Ramos, V. Vlassov, Theoretical analysis of low frequency temperature oscillation in a capillary pumped loop with porous element in the condenser, in: Proceedings of the 11th International Heat Pipe Conference, Tokyo, Japan, vol. 1, 1999, pp. 190–195.

[16] C.R. Gane, A.J. Oliver, D.R. Soulsby, P.L. Stephenson, Numerical solution of coupled conduction–convection problems using lumped-parameter methods, in: Proceedings of the Numerical Methods in Heat Transfer, vol. II, Wiley, New York, 1983, pp. 227–274.

[17] H. Schlichting, Boundary-Layer Theory, Mc-Graw-Hill, New York, 1968, pp. 560–592.